Supporting Information

3D super-resolution imaging with blinking quantum dots

Yong Wang,[1,2] Gilbert Fruhwirth,[3] En Cai,[1,2] Tony Ng,[4] and Paul R. Selvin[1,2,5,*]

[1]Department of Physics, [2]Center for the Physics of Living Cells, and [5]Center for Biophysics and Computational Biology, University of Illinois at Urbana-Champaign, Urbana, Illinois 61801, United States

[3]Department of Imaging Chemistry and Biology, Division of Imaging Sciences and Biomedical Engineering, St.Thomas' Hospital, London SE1 7EH, United Kingdom

[4]The Richard Dimbleby Department of Cancer Research, King's College London, London SE1 1UL, United Kingdom

[*]To whom correspondence may be addressed:
Paul R. Selvin
Telephone: (217) 244-3371
Fax: (217) 333-4898
Email: selvin@illinois.edu

Principle of QDB3. We illustrate the principle of QDB3 furthermore in SI Figure 5. We start with 11 quantum dots (SI Figure 5a, the same data from Figure 2). At some point, one quantum dot, QDi, blinks and goes to the off state (SI Figure 5b). Subtraction of SI Figure 5b from SI Figure 5a results in an intermediate image (SI Figure 5c, or with color-bar rescaled, SI Figure 5d). This intermediate image (SI Figure 5d) is the PSF of QDi. In other words, we isolate out the PSF of a single quantum dot. Fitting the PSF (SI Figure 5e) with a two-dimensional Gaussian (and applying the calibration curve) gives the position (x, y, z) of this quantum dot.

We note that there is a conceptual difference between the current method and SOFI[1] (or other methods such as 3B analysis[2] or faster STORM using compressed sensing[3]). For example, SOFI calculates mathematical quantities, such as cumulant correlation functions or variance of various orders. The intensities of pixels in the resultant SOFI images are assigned with the values from these mathematical quantities[1,4]. In other words, individual quantum dots are not localized at all. In contrast, in the current method, if a quantum dot undergoes a transition between on and off states (on → off, or off → on), the intensity and point spread function (PSF) of this quantum dot will be calculated by subtracting adjacent frames before and after the transition. The PSF (and intensity) of this single quantum dot can then be localized with high precision.

By applying the algorithm repeatedly on a movie, we can get a series of intermediate images (SI Figure 6, or an intermediate movie), isolate the PSFs of the quantum dots in the diffraction-limited spot and localize them one by one with high precision. At the end, we can then reconstruct the super-resolution image.

Another way to help to understand the principle of the current method (and why the resolution is improved compared to SOFI of the 25th order) is to think about the intermediate movie as the raw data obtained in STORM/PALM microscopy. When a quantum dot undergoes a transition between the on/off states, it appears on the intermediate movie. Then the transition can be viewed as the "*activation*" of the quantum dot in the intermediate movie. Note that the blinking of quantum dots is stochastic and thus the "*activation*" is also stochastic. This point is shown in SI Figure 7, which is from the same data in Figure 7. Here we focus on a small region (SI Figure 7b, rectangular area in SI Figure 7a). An intermediate movie is generated as described above and a few frame of the intermediate movie is shown in SI Figure 7c to 7e.

On each frame, only a subset of the quantum dots is "*activated*", similar to STORM/PALM. Bearing this in mind, it is reasonable that we achieved resolutions similar to (slightly better than, in x-y plane, presumably due to the fact that quantum dots are brighter) the values with STORM[5], but 3-7 times better than SOFI[1].

Resolution of QDB3. First we achieved ~1 nm for the precision for localizing a single quantum dot. The localization precision is determined by $\sigma_i = \sqrt{\frac{s_i^2}{N} + \frac{a^2}{12N} + \frac{8\pi s_i^4 b^2}{a^2 N^2}}$ where $i = x, y$, s_i is the standard deviation of the 2D Gaussian fitting of the point spread function (PSF), N is the total number of collected photons, a is the pixel size, and b is the standard deviation of background [6,7]. An example of one quantum dot is shown in SI Figure 8, where $N = 19291$, $a = 100$ nm, $b = 26.9$, $s_x = 104.5$ nm, $s_y = 108.9$ nm and we achieved $\sigma_x = 1.1$ nm, $\sigma_y = 1.2$ nm for localization precision.

To quantify the resolution that QDB3 can achieve, we first looked at individual quantum dots immobilized on a coverslip. Each quantum dot blinks for multiple times, allowing localization for multiple times, resulting in a cluster of localizations, as shown in SI Figure 9. Histograms of the distribution in x, y, and z were fit to Gaussian functions, yielding standard deviations of $\sigma_x = 2.4 \pm 0.4$ nm in x, $\sigma_y = 7.1 \pm 0.7$ nm in y, and $\sigma_z = 32.1 \pm 1.2$ nm in z.

To improve the statistics, similar to Ref 5, the localizations from many clusters (588 quantum dots) were aligned by their center of mass to generate the overall 3D presentation of the localization distribution (Figure 1b). Histograms of the distribution in x, y, and z were fit to Gaussian functions, yielding standard deviations of $\sigma_x = 3.7 \pm 0.0$ nm in x, $\sigma_y = 6.6 \pm 0.0$ nm in y, and $\sigma_z = 24.6 \pm 0.4$ nm in z (Figure 1c – e), corresponding to resolutions (fwhm = 2.35 σ) in the three directions of 8.7, 15.5 and 57.8 nm. Compared to the 25th-order SOFI imaging, which also used quantum dots and achieved fwhm resolution of 55 nm in x-y plane[1], the resolution of QDB3 is ~ 4-7 fold higher. Similarly, z-resolution of QDB3 is ~ 7 times better than that from the 16th order SOFI[1]. As we mentioned above, intermediate movies generated in this method can be viewed as the raw data obtained in STORM/PALM microscopy. On each frame, only a small subset of quantum dots (i.e., the ones undergo stochastic transitions) is "*activated*". Bearing this in mind, it is reasonable that we achieved resolutions similar to the values from STORM[5], but a few times better than SOFI[1].

In addition, we examined the resolutions for localizing quantum dots deep in solution. We prepared a sample of quantum dots on the surfaces of 1260 nm beads as illustrated below but with reduced concentration of quantum dots and reduced incubation time (5 minutes), such that individual quantum dot on beads can be seen. SI Figure 10 shows an example of a bead (gray scale, bright field), on top of which several quantum dots are shown in red. To make sure that we localize the same single quantum dot (i.e., there is only one quantum dot in an 8-pixel by 8-pixel area), the intensity traces of the quantum dots are examined. Only the quantum dots (indicated by yellow arrow) showing clearly two states (SI Figure 10b) are used for analysis. We note that it is in practice very difficult to have only one quantum dot (physically) on one bead. Based on our observation, a bead either has no quantum dot, or several quantum dots; only one bead out of >100 beads has one quantum dot physically.

We first confirmed that the localization precision, determined by $\sigma_i = \sqrt{\frac{s_i^2}{N} + \frac{a^2}{12N} + \frac{8\pi s_i^4 b^2}{a^2 N^2}}$ [6,7], of individual quantum dot on the surfaces of beads is still ~ 1 nm (0.9-1.8 nm). Then we determined 3D localization distribution of quantum dots on beads as we did for quantum dots on a coverslip. We achieved $\sigma_x = 3.3 \pm 0.1$ nm in x, $\sigma_y = 7.2 \pm 0.5$ nm in y, and $\sigma_z = 34.6 \pm 1.3$ nm in z (corrected for refractive index mismatch), as shown in SI Figure 11. The resolution in x-y plane does not change much; but the resolution in z is slightly higher, compared to the z-resolution for quantum dots on a coverslip surface. Nonetheless, compared to the 25th order SOFI imaging, the x-y resolution of QDB3 is 3-7 folds better; and z- resolution of QDB3 (on beads) is ~ 5 times better than that from the 16th order SOFI [1].

Preparation of spherically distributed quantum dots. Coverslips were first cleaned in 10 M KOH with sonication for 20 minutes, rinsed with ddH_2O, dried with nitrogen, and burned with a propane torch. The surfaces of the cleaned coverslips were then derived with amino-silane and coated with Polyethylene glycol polymers (PEG), 2% of which were functionalized with biotin at the end. The use of PEG surface minimized non-specific binding of quantum dots on the coverslip. After rinsing with ddH_2O, the coverslips were dried with nitrogen and used to make flow chambers, giving chamber-volumes of ~ 10 uL. Polystyrene beads, coated streptavidin (SVP-10-5 or SVP-05-10, Spherotech Inc., IL), were added to the chamber at concentrations of 1.5 – 3.6 pM and were immobilized on the functionalized coverslips through streptavidin-biotin interactions. After 30 minutes of incubation at room temperature, the chamber was washed with PBS. Quantum dots were then labeled with biotin (Q10301MP, Life Technologies Corp., CA) and added to the chambers and immobilized on the beads. This was then incubated in a wet box at room temperature overnight. After washing with PBS, the samples were used for imaging.

Labeling of EGFR on breast cancer cell.

Cell culture. The triple-negative human ductal carcinoma cell line HCC1143 was obtained from ATCC. Breast cancer cells were cultured in RPMI 1640 medium (PAA, Farnborough, UK) containing 4.5g/L glucose, 2mM L-glutamine, 1mM sodium pyruvate, 10mM HEPES, and 1.5g/L sodium bicarbonate, which was supplemented with 10% fetal calf serum (BioSera, Uckfield, UK), in an atmosphere containing 5% CO2 (v/v) at 37°C. Subculturing was performed by removing the growth medium, washing the cells with phosphate buffered saline without calcium or magnesium (PBS), and incubating the cells with 0.25% trypsin (PAA, Farnboroug, UK) and 0.53mM EDTA until cell detachment at 37°C. Subsequently, cells were aspirated, spun at 200g for 5min, the supernatant was discarded, the cell pellet resuspended in growth medium, and cells were seeded into new culture flasks (subcultivation ratio was 1:4) or onto glass cover slips for experiments.

Formation of EGF-biotin:streptavidin-QDot complexes. The complexes were formed via a modified protocol based on the method of Lidke et al[8] and prepared freshly for every experiment. Briefly, EGF-biotin (500nM) was added slowly under stirring to streptavidin-QDots (500nM in respect to QDots) and incubated for 30min at 4°C while mixing (molar ratio 1:1). Samples were purified by size exclusion chromatography over P-30 spin columns (BioRad, Hemel Hempstead, UK) but no unbound EGF-biotin was detected (using a fluorescence-based biotin quantitation kit (Thermo Fisher Scientific, Northumberland, UK)) suggesting all EGF-biotin was bound to streptavidin-QDots. Subsequently, complexes were diluted to working concentrations and used to treat cells as indicated.

Cell treatments and sample preparation. Cells were grown on acid-treated and autoclaved glass coverslips to the desired cell densities. Subsequently, cells were treated with 4nM pre-formed EGF-biotin:streptavidin-QDot complexes in growth medium at 37°C for the indicated times. The specific type of QDot used and its emission wavelength is indicated accordingly in the results and figures section. After treatment, the cells were three times washed with ice-cold Tris-buffered saline (TBS) and then fixed in 4%

(w/v) paraformaldehyde (PFA) in TBS for 15 min. After two final washing steps each with TBS and distilled water, samples were mounted in Mowiol 4-88 (Polysciences Inc., Warrington, PA, U.S.),, which was intended to match the refractive index of immersion oil, and left to dry in the dark at RT overnight. If desired, DTT (10mM) as a reducing agent was added to the mounting medium.

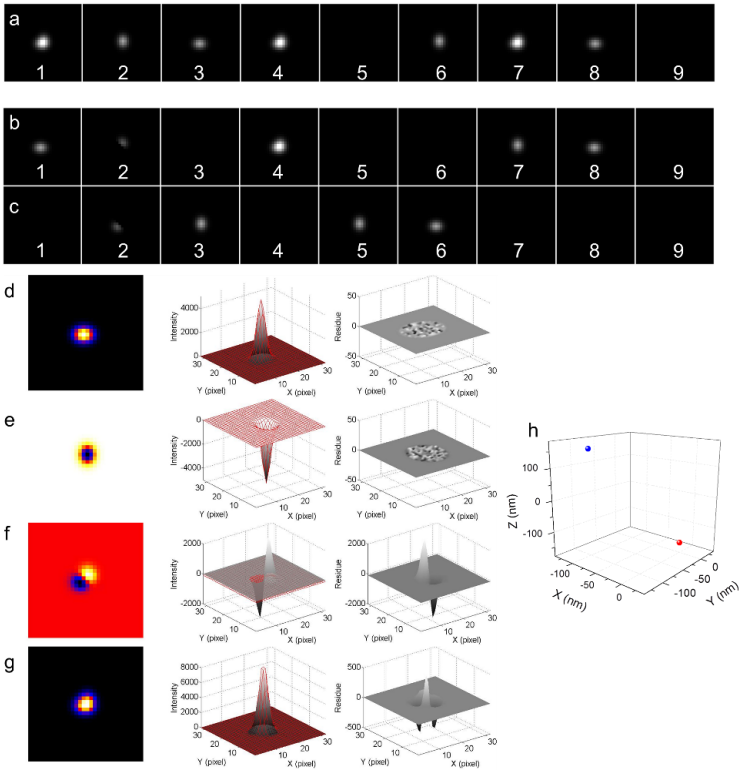

SI Figure 1. Principle of QDB3. (a) The original movie of two quantum dots. (b-c) Two intermediate movies, created by subtracting adjacent frames in both backward and forward directions. (d-g) Four different types of PSFs present in the intermediate movies. The PSFs are fitted by Gaussian functions and the residues of the fitting are also plotted. (h) The three dimensional positions of the two quantum dots determined by QDB3, based on a calibration curve measured experimentally and the ellipticity of the fitted elliptical Gaussian functions.

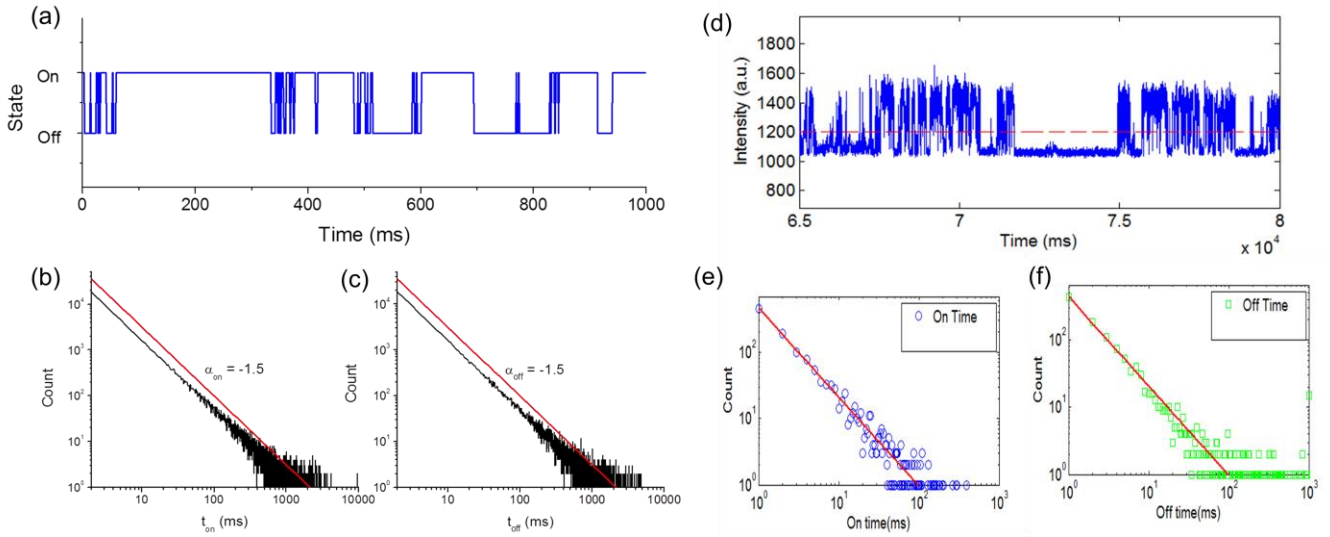

SI Figure 2. Blinking of simulated quantum dots and real quantum dots. (a) An example of the trace of a quantum dot used in simulated movies is shown. The probabilities of the on-time (b) and off-time (c) obey a power law: $P(t) \propto t^{-\alpha}$, where α_{on} = -1.5 and α_{off} = -1.5 (red lines with slopes of -1.5 are shown). (d) An example of the intensity trace of a real quantum dot used in the experiments (measured at temporal resolution of 1 ms). It is confirmed that the probabilities of the on-time (e) and off-time (f) follow power-laws.

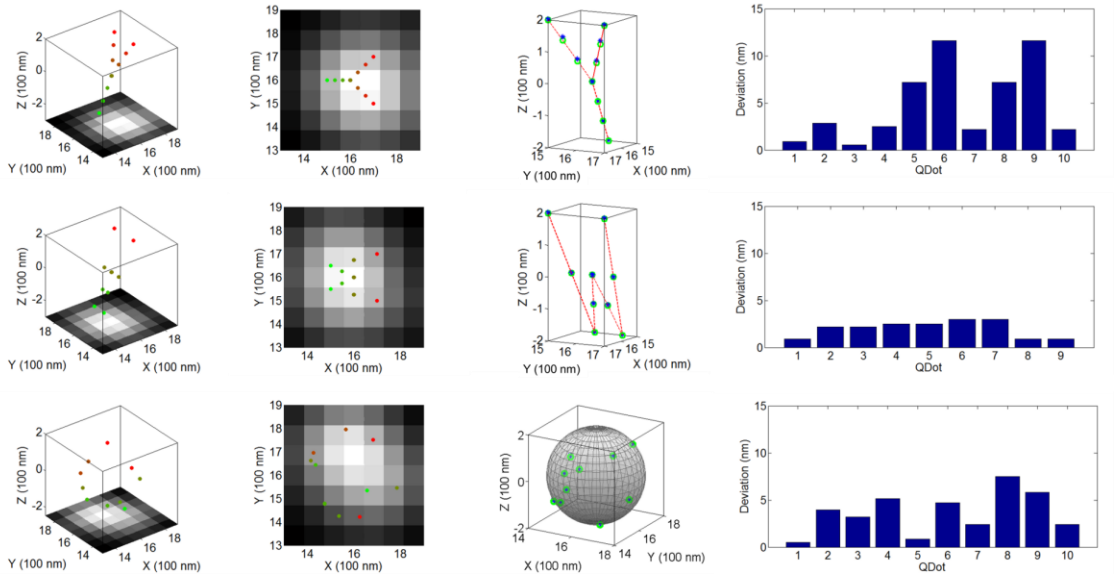

SI Figure 3. Three-dimensional images obtained by QDB3 from simulated movies of quantum dots with patterns of a letter Y (top), a letter W (middle) and a random spherical distribution (bottom) in the absence of noise.

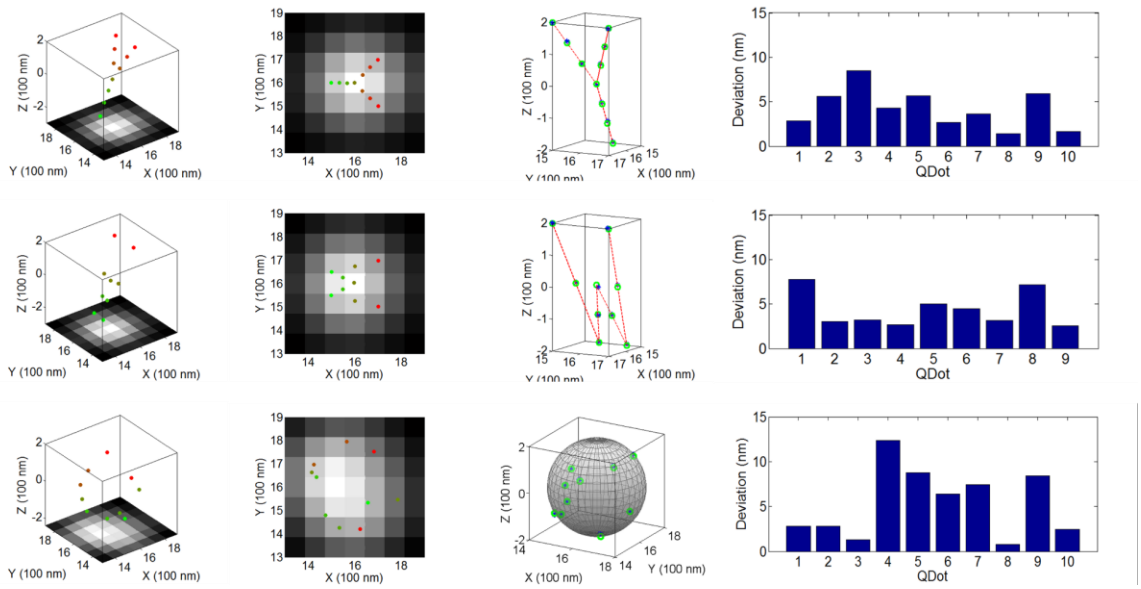

SI Figure 4. Three-dimensional images obtained by QDB3 from simulated movies of quantum dots with patterns of a letter Y (top), a letter W (middle) and a random spherical distribution (bottom) in the presence of Poisson noises.

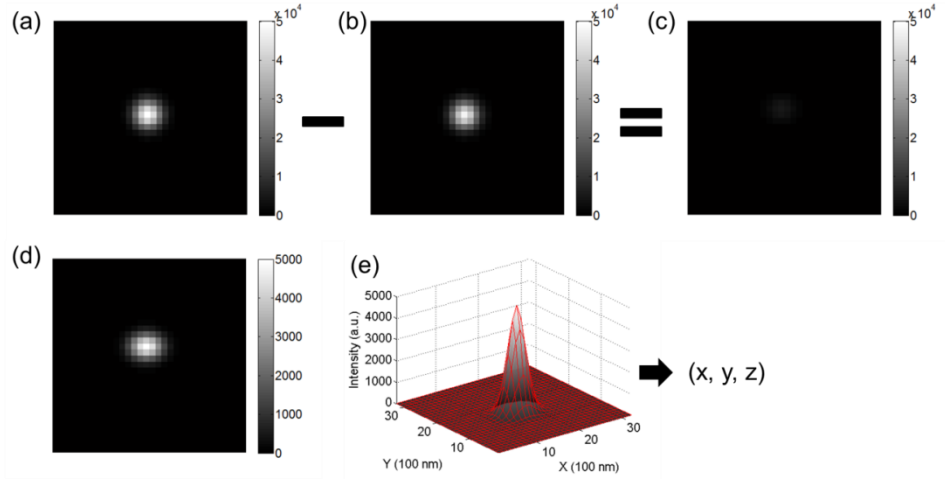

SI Figure 5. (a) Simulated image of 11 quantum dot: 11 are on; (b) Simulated image of the same 11 quantum dots in (a) but one of the quantum dot undergoes a transition from on to off: 10 are on while 1 is off; (c) Subtraction of (b) from (a) results in the PSF of the single quantum dot in the off state; (d) Same as (c) but the color-bar is rescaled; (e) Two-dimensional Gaussian fitting of (d) gives the position of the quantum dot.

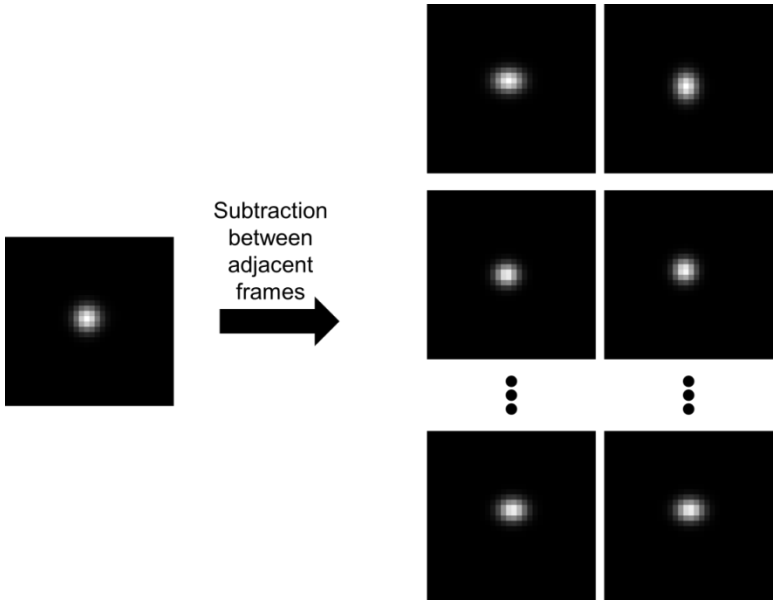

SI Figure 6. Repeating the process in SI Figure 5 on a movie (left) gives a series of intermediate images (right), consisting of an intermediate movie.

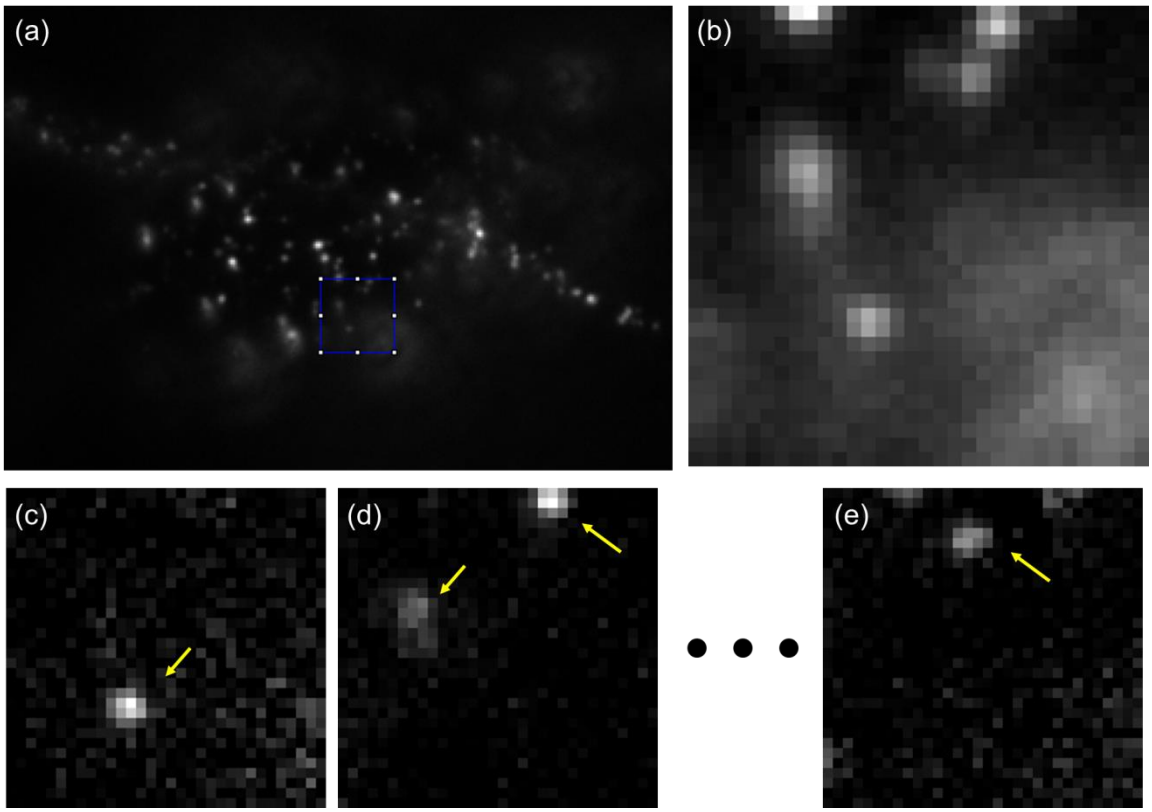

SI Figure 7. (a) Image from a breast cancer cell using normal fluorescent microscopy (from real data shown in Figure 7a); (b) Zoom-in of the rectangular region in (a); (c-e) A few frames from the intermediate movie show "*activated*" quantum dots.

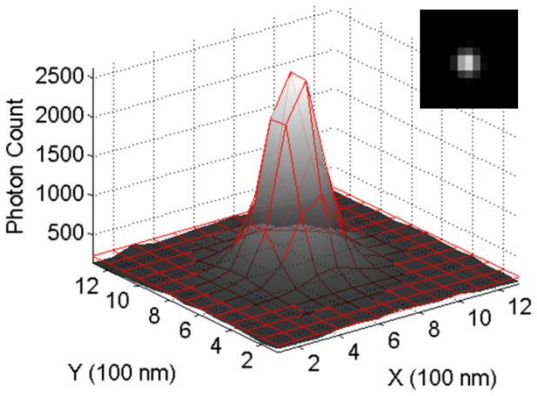

SI Figure 8. Localization with ~ 1nm precision of a quantum dot from a single blinking event (Inset: point spread function of the quantum dot). The localization precision is determined by $\sigma_i = \sqrt{\frac{s_i^2}{N} + \frac{a^2}{12N} + \frac{8\pi s_i^4 b^2}{a^2 N^2}}$ where s_i is the standard deviation of the 2D Gaussian fitting of the point spread function , N is the total number of collected photons, a is the pixel size, and b is the standard deviation of background [6,7]. For this specific example, we achieved $\sigma_x = 1.1\,\text{nm}$, $\sigma_y = 1.2\,\text{nm}$.

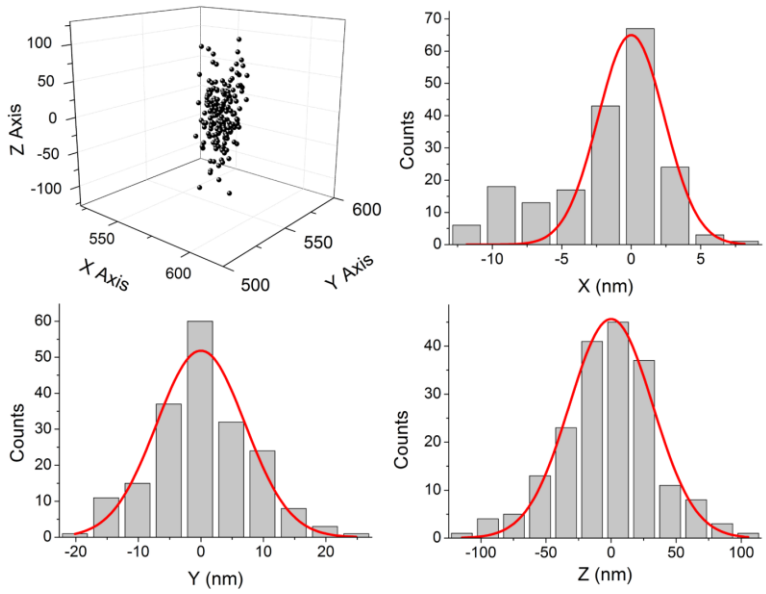

SI Figure 9. Three-dimensional localization distribution of a single quantum dot. The quantum dot blinks for multiple times, allowing localization for multiple times, resulting in a cluster of localizations. Histograms of the distribution in x, y, and z were fit to Gaussian functions, yielding standard deviations of $\sigma_x = 2.4 \pm 0.4$ nm in x, $\sigma_y = 7.1 \pm 0.7$ nm in y, and $\sigma_z = 32.1 \pm 1.2$ nm in z.

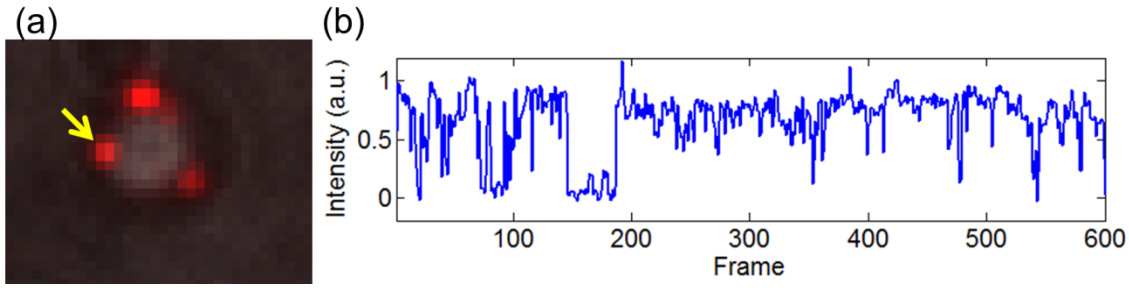

SI Figure 10. (a) Sample of quantum dots (red) on the surface of a bead (gray). (b) Intensity trace of the quantum dot, indicated by the yellow arrow in (a), showing two states.

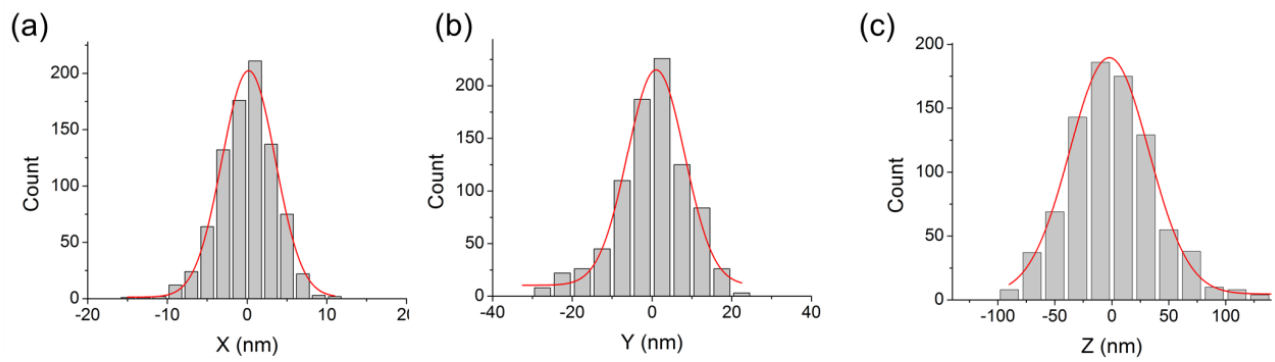

SI Figure 11. Histograms of the localization distribution in x, y, and z (from 5 quantum dots on surfaces of beads). The distributions were fitted to Gaussian functions, yielding standard deviations of $\sigma_x = 3.3 \pm 0.1$ nm, $\sigma_y = 7.2 \pm 0.5$ nm, and $\sigma_z = 34.6 \pm 1.3$ nm.

References

(1) Dertinger, T.; Colyer, R.; Iyer, G.; Weiss, S.; Enderlein, J. *PNAS* **2009**, *106*, 22287–22292.
(2) Cox, S.; Rosten, E.; Monypenny, J.; Jovanovic-Talisman, T.; Burnette, D. T.; Lippincott-Schwartz, J.; Jones, G. E.; Heintzmann, R. *Nat Meth* **2012**, *9*, 195–200.
(3) Zhu, L.; Zhang, W.; Elnatan, D.; Huang, B. *Nat Meth* **2012**, *9*, 721–723.
(4) Watanabe, T. M.; Fukui, S.; Jin, T.; Fujii, F.; Yanagida, T. *Biophysical Journal* **2010**, *99*, L50–L52.
(5) Huang, B.; Wang, W.; Bates, M.; Zhuang, X. *Science* **2008**, *319*, 810 –813.
(6) Thompson, R. *Biophysical Journal* **2002**, *82*, 2775–2783.
(7) Yildiz, A.; Forkey, J. N.; McKinney, S. A.; Ha, T.; Goldman, Y. E.; Selvin, P. R. *Science* **2003**, *300*, 2061 –2065.
(8) Lidke, D. S.; Nagy, P.; Heintzmann, R.; Arndt-Jovin, D. J.; Post, J. N.; Grecco, H. E.; Jares-Erijman, E. A.; Jovin, T. M. *Nature Biotechnology* **2004**, *22*, 198–203.